1992ApJ...399..563B

THE ASTROPHYSICAL JOURNAL, 399:563–572, 1992 November 10
© 1992. The American Astronomical Society. All rights reserved. Printed in U.S.A.

MID-INFRARED ROTATIONAL LINE EMISSION FROM INTERSTELLAR MOLECULAR HYDROGEN

MICHAEL G. BURTON,[1] D. J. HOLLENBACH,[2] AND A. G. G. M. TIELENS[2]
Received 1991 September 20; accepted 1992 May 15

ABSTRACT

We have modeled the line emission from the $v = 0$–0 $S(0)$, $S(2)$, and $S(3)$, and the $v = 1$–0 and $v = 2$–1 $S(1)$ transitions of molecular hydrogen in clouds exposed to high far-ultraviolet fluxes (i.e., photodissociation regions or PDRs) and in shocks. In particular, we have studied the lowest pure rotational H_2 transitions [the 0–0 $S(0)$ and 0–0 $S(1)$ lines], at 28 and 17 μm, respectively. We find that, in PDRs, the emission comes from warm ($T \gtrsim 100$ K) molecular gas, situated at optical depths $A_v \gtrsim 1$, beyond the hot atomic surface layer of the clouds. For FUV fields, $G_0 = 10^3$–10^5 times the average interstellar field and densities $n = 10^3$–10^7 cm^{-3}, the typical line intensities are in the range 10^{-6} to 10^{-4} ergs s^{-1} cm^{-2} sr^{-1}. We compare the predictions for the line intensities from both C-type and J-type shock models. For both nondissociative and dissociative molecular shocks, in the same density range, the line intensities range from 10^{-6} to 10^{-3} ergs s^{-1} cm^{-2} sr^{-1}. In the faster, dissociative shocks ($v_s \gtrsim 25$–30 km s^{-1}), the H_2 line emission arises from reformed molecules, downstream of the shock front. Shocked line emission may be detectable from lower velocity shocks (i.e., $v_s \sim 5$ km s^{-1}) than previously observed. Measurements of the relative line ratios may be used to help discriminate between competing models for the shock excitation of molecular gas. Observations of these lines will also provide a powerful probe of the extensive regions of warm molecular gas in the Galaxy. The results are applied to recent observations of the 0–0 $S(1)$ transition in both the PDR and the shocked gas in Orion. The *Infrared Satellite Observatory* (*ISO*) should detect the $v = 0$–0 low-J transitions in numerous active regions.

Subject headings: infrared: interstellar: lines — ISM: molecules — molecular processes — shock waves

1. INTRODUCTION

Line emission from the rotational and vibrational levels of the ground electronic state of molecular hydrogen (H_2) occurs at wavelengths extending from the UV to the far-IR. The vast majority of these lines are far too weak to be detectable, and the study of H_2 line emission from the interstellar medium has concentrated on the near-IR spectrum, from 1 to 5 μm, with limited observations outside this regime. Most lines observed result from changes in the vibrational quantum number, $\Delta v \sim 1$–3, and arise from energy levels >6000 K above the ground state. Excitation temperatures above 1000 K and densities $\gtrsim 10^4$ cm^{-3} are required in order to collisionally populate the upper levels of the transitions. Alternatively, and often more prominently, these rovibrational bands can be pumped through UV photons (e.g., Black & van Dishoeck 1987). The behavior of the ground-state transitions of the molecule is somewhat different. The two lowest para and ortho transitions, the $v = 0$–0 $S(0)$ and $S(1)$ lines, at 28.2 and 17.0 μm, respectively, arise from levels only 510 and 1015 K above ground. They can therefore be excited at much cooler temperatures than the vibrational lines. In addition, they have low critical densities. For instance, at 200 K, the critical densities (for collisions with atomic hydrogen) for these transitions are ~ 10 and 300 cm^{-3}, respectively. These mid-IR lines are, however, difficult to observe due to the large thermal background and poor atmospheric transmission at their emission wavelengths. Moreover, they are intrinsically weak due to their low radiative decay rates ($\tau_{\rm decay} \gtrsim 100$ yr). Yet they hold the potential of being powerful probes of the extensive regions of warm ($\gtrsim 100$ K) molecular gas which exist in the Galaxy. They are optically thin lines, originating from the bulk of the gas present, and not from trace constituents, such as the CO $J = 1$–0 line, which has commonly been used to probe molecular clouds.

In this paper we discuss the $v = 0$–0 $S(0)$, $S(1)$, $S(2)$, $S(3)$, 1–0 $S(1)$ and 2–1 $S(1)$ line emission from photodissociation regions (PDRs) and shocks, the two principal environments where H_2 line emission has been observed. The focus is on the 0–0 $S(0)$ and $S(1)$ lines of the molecule. The impetus for this work comes from the recent detection by Parmar, Lacy, & Achtermann (1991) of the 0–0 $S(1)$ line in the Orion Bar, and from the imminent launch of the *Infrared Satellite Observatory* (*ISO*) with the promise of detecting both the ground-state 0–0 $S(0)$ line and the 0–0 $S(3)$ line for the first time.

Neutral clouds irradiated by far-ultraviolet (FUV) photons are known as photodissociation regions (PDRs; e.g., Tielens & Hollenbach 1985a, hereafter TH). The heating of the gas occurs by photoelectrically ejected electrons from grain surfaces colliding with the gas particles. Emission from such regions is dominated by far-infrared (FIR) thermal continuum from dust grains, and by atomic fine structure and molecular line emission. Near-infrared vibrational transitions of fluorescently excited molecular hydrogen (H_2), pumped by the UV photons, originate in the warm, mainly atomic, surface zones of these clouds ($T \sim 500$ K, $A_v \lesssim 2$) (e.g., Black & van Dishoeck 1987). If the gas density is sufficiently high ($n \gtrsim 10^5$ cm^{-3}), however, substantial amounts of warm, thermalized H_2 are produced, leading to observable quantities of collisionally excited H_2 line emission (e.g., Sternberg & Dalgarno 1989; Burton, Hollenbach, & Tielens 1990b, hereafter BHT). These latter two papers present detailed models for the molecular gas in dense PDRs, but their discussions on H_2 line emission concentrated on the near-IR vibrational lines, which come from levels whose ener-

[1] Anglo-Australian Observatory, Epping Laboratory, P.O. Box 296, Epping, N.S.W. 2121, Australia.
[2] Mail Stop 245-3, Space Science Division, NASA/Ames Research Center, Moffett Field, CA 94035.

© American Astronomical Society • Provided by the NASA Astrophysics Data System

1992ApJ...399..563B

gies are >6000 K above the ground. The emission from the 0–0 $S(0)$ and $S(1)$ lines arises deeper into the cloud than the vibrational lines, where the hydrogen is mainly molecular, rather than from the neutral atomic surface layer.

Molecular shock waves also heat the gas and excite the rotational and vibrational lines of H_2 (e.g., Hollenbach & Shull 1977; Kwan 1977; London, McCray, & Chu 1977; Beckwith et al. 1978; Draine & Roberge 1982; Chernoff, Hollenbach, & McKee 1982; Draine, Roberge, & Dalgarno 1983; Flower, Pineau des Forêts, & Hartquist 1985; Brand et al. 1988; Burton et al. 1989a, b; Hollenbach & McKee 1989; Chang & Martin 1991; Smith 1991). There are two classes of molecular shock, C- and J-type, and both produce significant H_2 line emission. C-type shocks (cf. Draine 1980) are magnetized, non-dissociative molecular shocks in which the neutrals are heated by ambipolar diffusion of the trace ions. In J-type shocks, viscous heating of the neutrals occurs in a shock front in which radiative cooling is insignificant, thereby permitting the treatment of the front as a discontinuity with the Rankine-Hugoniot jump conditions. We have performed new calculations of the H_2 spectra from nondissociative J-shocks for this paper, and, for convenience, review previous results from C-shocks and dissociative J-shocks. Due to their lower energy levels, the 0–0 $S(0)$ and $S(1)$ lines can be excited by somewhat slower shocks than the observed near-IR H_2 lines.

The PDR and shock modeling is described in § 2, followed by the results and discussion in § 3. In addition to predicting H_2 intensities and line ratios, we discuss the calculation of the ortho-to-para ratio in the emitting gas, and the prospects for a direct determination of the CO/H_2 abundance ratio from observations of the H_2 17 and 28 μm lines and rotational CO lines. Some applications to the observation of rotational emission are given in § 4. This includes a comparison with the recent detection of the 17 μm line in the Orion Bar and the Orion shock, and a discussion of future prospects for their detection, particularly with ISO. The conclusions are in § 5.

2. MODELING

2.1. *Photodissociation Regions*

This section extends the PDR models of both TH and BHT. The models represent the chemistry and energy balance of a cloud exposed to an external FUV flux as a function of optical depth from the neutral surface. As such, they represent the one-dimensional emission from a PDR seen face-on. The heating, cooling, and chemistry of H, He, C, O, Si, S, Fe, and Mg species is treated iteratively from the neutral surface into the cloud interior. The main free parameters are the gas density, n, and the FUV field, G_0, where G_0 is measured in units of the local interstellar radiation field (taken to be equivalent to a one-dimensional flux of 1.6×10^{-3} ergs s^{-1} cm^{-2} in the 6–13.6 eV band; Habing 1968). Models were run covering the parameter space for n from 10^3 to 10^7 cm^{-3}, and for G_0 from 10^3 to 10^5. For other details the reader is referred to TH and BHT.

In particular, the emission from the $v = 0$, $J = 2$, 3, 4, and 5 levels was followed, by calculating, at each optical depth step, the statistical equilibrium population of the H_2 levels for the gas temperature, density, and H_2 abundance. In practice, this was negligibly different from the populations determined for the $J = 2$ and 3 levels if LTE was assumed, for the parameter space explored. These level populations are therefore determined by collisions and not UV-pumping. An ortho-to-para ratio of 3:1 was assumed. Neutral collisions and radiative decay proceed with ΔJ even, thereby conserving ortho- and para-H_2. We ignore ortho-to-para conversion by H^+ and by H exchange. This point is discussed further in § 3.1.2. Since the H_2 line emission is optically thin, the intensities of the 0–0 $S(0)$ line at 28.221 μm and the 0–0 $S(1)$ line at 17.035 μm can be calculated directly from the column densities in the excited energy levels.

2.2. *Shock Waves*

The J-shock code of Hollenbach & McKee (1989) and of Brand et al. (1988) was used to calculate the H_2 spectrum of nondissociative J-shocks. The former code incorporates a fairly elaborate chemical network which follows the abundances of 35 chemical species in the hot, compressed postshock gas. Especially important is the formation of H_2O (see later), which can dominate the cooling for preshock densities of $n_0 \gtrsim 10^5$ cm^{-3}. All gas phase oxygen not incorporated in CO tends to be converted to H_2O in the warm ($T > 300$ K) postshock gas. The Hollenbach & McKee code also follows the statistical equilibrium of the H_2 levels, and the change in γ, the specific heat, as the rotational and vibrational levels of the H_2 molecule are excited. For the model runs of the Hollenbach & McKee code we have taken initial conditions identical to those which Draine et al. (1983) adopted in their C-shock models. These are listed in Table 1. The ortho-to-para ratio of H_2 is held fixed at a value of 3:1; see § 3.2.2 for a discussion of this assumption.

The Brand et al. (1988) model is a simpler, semianalytic code which assumes that the H_2 dominates the cooling (through both line cooling and molecule dissociation), that H_2 is in LTE, and that $\gamma = 7/5$. H_2O line emission is assumed to be negligible, and molecule reformation is neglected. We present the results because Brand et al. have argued that nondissociative J-shocks may provide the best fit to the observed H_2 spectrum in a number of sources, but especially in the OMC-1 shock. The results may be regarded as representative of observations of H_2 emission from dense molecular shocks dominated by H_2 cooling. We note, however, that on theoretical grounds, most nondissociative molecular shocks would be expected to be C-shocks unless ionization fractions are high and magnetic fields are weak (see, for example, Hollenbach, Chernoff, & McKee 1989).

The neglect of H_2O cooling in the Brand et al. model might be regarded as an extreme and rather ad hoc assumption. It is,

TABLE 1

INITIAL CONDITIONS FOR SHOCK MODELS

Density	Parameter	Value
All n	CO	1.00 (−4)
	O	3.75 (−4)
$n = 10^4$ cm^{-3}	H	3.05 (−4)
	e	1.00 (−7)
	B_0	50 μG
$n = 10^6$ cm^{-3}	H	3.05 (−6)
	e	1.00 (−8)
	B_0	500 μG

NOTE.—Listed here are the initial abundances of certain species, and transverse magnetic field, B_0. Initially all carbon is assumed to be in CO, and all oxygen not in CO is in O. All hydrogen is in H_2 except for the initial trace H abundance listed here.

© American Astronomical Society • Provided by the NASA Astrophysics Data System

1992ApJ...399..563B

however, symptomatic of our current lack of understanding of the behavior of molecular shocks, an issue beyond the scope of this paper (but see, for instance, Hollenbach et al. 1989 and Draine 1991). Nevertheless the Brand et al. model provides an excellent fit to the H_2 data from OMC-1, and there is some evidence to suggest that H_2O line emission is less than the C-shock predictions. Certainly the H_2O line intensities predicted by the C-shock model of Neufeld & Melnick (1987) have not been substantiated by observation, although this is a hard experiment to conduct. For the SNR IC 443, a similar J-shock model to Brand et al. reproduces the observed H_2 and [O I] 63 μm line intensities (Burton et al. 1990a), with little H_2O line emission predicted. Moreover comparison with the *IRAS* 60 μm band emission provides upper limits on the total H_2O line emission that could be produced by the shock.

3. RESULTS AND DISCUSSION

3.1. *PDRs*

Figure 1 shows the ratio of the low-J H_2 lines as a function of temperature for gas in LTE. As can be seen, these line ratios are most sensitive as diagnostics for temperatures $\lesssim 400$ K. We note that, although the $S(1)/S(0)$ line ratio is the most sensitive ratio for probing cooler gas, it depends on the ortho-to-para ratio. This in turn depends on the ortho-to-para conversion efficiency; if it is high, the ratio is the LTE value, which drops significantly below 3 for $T \lesssim 200$ K. However, although the efficiency is low, we note that non–LTE values of <3 might still be achieved. The ortho-to-para ratio appropriate for a particular line will depend on the depth into the PDR where the bulk of its emission occurs. This is discussed further in § 3.1.2. Figure 1 assumes an ortho-to-para ratio of 3.

3.1.1. H_2 *Line Fluxes*

Figure 2 provides a method of estimating the flux of a given line. Shown is the line intensity divided by the hydrogen nucleus column density in units 10^{21} cm^{-2}, $N_{21} = N/10^{21}$ cm^{-2}, assuming LTE. Typically, the bulk of the H_2 line emission comes from $\Delta A_v \sim 1$, corresponding to a column of gas $\sim 2 \times 10^{21}$ cm^{-2}. For temperatures 100–350 K, the 0–0 $S(1)$ line is the brightest line in the emitting gas, and the 0–0 $S(3)$ line dominates for temperatures from 350 to 1000 K. At higher temperatures, rotational-vibrational transitions, such as the commonly observed 1–0 $S(1)$ line, are the brightest lines.

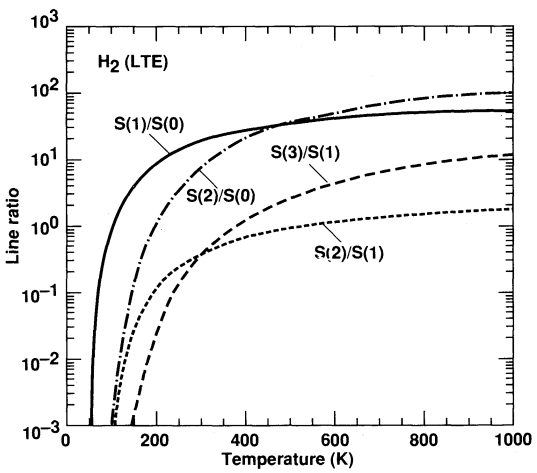

FIG. 1.—Line ratios for the lowest rotational H_2 lines as a function of temperature, for gas in thermal equilibrium and for a fixed ortho-to-para ratio of 3:1. Shown are the $v = 0$–0 $S(1)/S(0)$ (*solid curve*), $S(2)/S(0)$ (*dot-dash*), $S(2)/S(1)$ (*short dashes*), and $S(3)/S(1)$ (*long dashes*) line ratios.

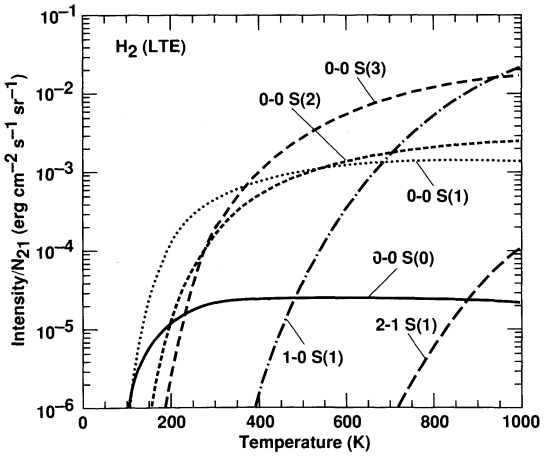

FIG. 2.—H_2 intensities for the $v = 0$–0 $S(0)$ (*solid curve*), $S(1)$ (*dots*), $S(2)$ (*short dash*), $S(3)$ (*middle dash*), $v = 1$–0 $S(1)$ (*dash-dot*), and $v = 2$–1 $S(1)$ (*long dash*) lines, as a function of temperature, for gas in LTE and fixed ortho-to-para ratio of 3:1. The y-axis is the line intensity, in ergs s^{-1} cm^{-2} sr^{-1}, divided by the hydrogen nucleus column density in units of 10^{21} cm^{-2}, $N_{21} = N/10^{21}$ cm^{-2}. By multiplying by the column of excited gas, in units of N_{21}, the specific intensity of a particular line may be obtained (see text).

In Table 2 are presented the results of the PDR model runs. Listed are the intensities of the 0–0 $S(0)$, $S(1)$, $S(2)$, and $S(3)$ lines, together with relevant physical parameters for the lines. For comparison purposes, the intensities of the 1–0 $S(1)$ and 2–1 $S(1)$ lines are also shown. (For $G_0 = 10^3$, two sets of figures are given in the table for $n = 10^6$ and 10^7 cm^{-3}, corresponding to the high-temperature and low-temperature solutions discussed by BHT. For these particular parameters, two stable solutions exist: the low-temperature solution for the conventional PDR where cooling through the [O I] 63 μm line balances photoelectric heating, and the high-temperature solution where cooling through gas-grain collisions balances H_2 vibrational heating close to the surface.) The excitation temperature, calculated from the ratio of the $S(0)$ and $S(1)$ line intensities, is also listed. Since the emission is coming from gas in LTE, this can be regarded as representative of the temperature where the bulk of the line emission occurs. This ranges from ~ 100 to ~ 300 K, rising as both the FUV field and density are increased. Figure 3 shows the results graphically for $n = 10^4$ and 10^6 cm^{-3}.

In general, it can be seen that 17 and 28 μm line intensities for these PDRs are a few times 10^{-6} to 10^{-4} ergs s^{-1} cm^{-3} sr^{-1}. The 0–0 $S(1)$ line is a few times brighter than the 0–0 $S(0)$ line for $G_0 = 10^3$ and an order of magnitude larger for the warmer gas produced when $G_0 = 10^4$–10^5. The 0–0 $S(1)$ line intensity is comparable to that of the 1–0 $S(1)$ line, and the 0–0 $S(0)$ intensity to that of the 2–1 $S(1)$ line, over much of the parameter space.

There are three contributions to H_2 line intensities in PDRs; UV pumping, collisional excitation, and H_2 formation. For the parameter space studied, the $v = 0$, $J = 2$ and 3 levels are in thermal equilibrium at the gas temperature, since the critical densities for these levels are $<10^3$ cm^{-3}. UV pumping and H_2 formation can be ignored as directly affecting the populations, although the energy released from these processes helps to heat the gas. Therefore, the 0–0 $S(0)$ and 0–0 $S(1)$ line intensities can

© American Astronomical Society • Provided by the NASA Astrophysics Data System

1992ApJ...399..563B

TABLE 2

MOLECULAR HYDROGEN LINE INTENSITIES IN PDRs

		LINE INTENSITY (ergs s^{-1} cm^{-2} sr^{-1})						
n[a]	G[b]	0–0 $S(0)$ 28.221 μm[c] 510 (K)[d] 2.94 (−11) s^{-1}[e]	0–0 $S(1)$ 17.035 μm[c] 1015 (K)[d] 4.76 (−10) s^{-1}[e]	0–0 $S(2)$ 12.279 μm[c] 1682 (K)[d] 2.76 (−9) s^{-1}[e]	0–0 $S(3)$ 9.665 μm[c] 2504 (K)[d] 9.84 (−9) s^{-1}[e]	1–0 $S(1)$ 2.1218 μm[c] 6952 (K)[d] 3.47 (−7) s^{-1}[e]	2–1 $S(1)$ 2.2477 μm[c] 12551 (K)[d] 4.98 (−7) s^{-1}[e]	EXCITATION TEMPERATURE[f] (K)
3	3	1.4 (−6)	3.1 (−6)	2.5 (−7)	6.0 (−7)	2.4 (−6)	1.4 (−6)	130
4	3	3.6 (−6)	1.5 (−5)	8.7 (−7)	1.0 (−6)	1.2 (−5)	6.8 (−6)	150
5	3	3.2 (−6)	1.0 (−5)	4.1 (−7)	6.5 (−7)	3.1 (−5)	1.9 (−5)	140
6	3a[g]	9.8 (−7)	1.2 (−6)	4.8 (−8)	1.8 (−7)	4.2 (−5)	2.5 (−5)	110
6	3b[g]	9.9 (−7)	3.1 (−6)	1.9 (−6)	6.6 (−6)	3.6 (−5)	2.1 (−5)	140
7	3a[g]	3.8 (−7)	2.8 (−7)	7.1 (−9)	3.0 (−8)	3.5 (−5)	2.1 (−5)	100
7	3b[g]	4.1 (−7)	1.9 (−6)	1.6 (−6)	5.6 (−6)	2.8 (−5)	1.7 (−5)	160
3	4	4.4 (−6)	1.6 (−5)	7.1 (−7)	6.5 (−7)	2.7 (−6)	1.6 (−6)	150
4	4	7.9 (−6)	5.7 (−5)	6.3 (−6)	3.0 (−6)	1.4 (−5)	8.5 (−6)	180
5	4	1.2 (−5)	1.3 (−4)	2.7 (−5)	2.3 (−5)	6.1 (−5)	2.7 (−5)	220
6	4	1.4 (−5)	2.3 (−4)	1.5 (−4)	5.0 (−4)	1.8 (−4)	2.7 (−5)	260
7	4	1.3 (−5)	2.9 (−4)	2.2 (−4)	7.6 (−4)	1.4 (−4)	1.8 (−5)	310
3	5	7.9 (−6)	3.8 (−5)	2.0 (−6)	8.6 (−7)	2.9 (−6)	1.7 (−6)	160
4	5	1.4 (−5)	1.3 (−4)	2.0 (−5)	1.1 (−5)	1.5 (−5)	9.0 (−6)	200
5	5	1.9 (−5)	3.0 (−4)	1.3 (−4)	2.6 (−4)	4.8 (−5)	1.5 (−5)	260
6	5	1.7 (−5)	3.7 (−4)	2.7 (−4)	9.3 (−4)	4.8 (−4)	2.9 (−5)	310
7	5	1.8 (−5)	4.2 (−4)	3.5 (−4)	1.4 (−3)	9.9 (−4)	8.7 (−5)	320

[a] Log of density, n, in cm^{-3}.
[b] Log of FUV field, G_0, in units of the average interstellar radiation field (Habing 1968).
[c] Wavelengths from Dabrowski 1984.
[d] Upper state levels from Dabrowski 1984.
[e] Radiative decay rates from Turner, Kirby-Docken & Dalgarno 1977.
[f] Excitation temperature derived from ratio of the 0–0 $S(0)$ and 0–0 $S(1)$ lines.
[g] Line intensities given for both low- (a) and high- (b) temperature solutions (see text).

simply be determined by knowledge of the temperature profile, density, and fractional H_2 abundance through the PDR. The bulk of the emission comes from gas with $T \sim T_{ex} = 100$–300 K, as listed in the last column of Table 2. More precisely, the thermal contribution, $I_{thermal}$, is given by

$$I_{thermal} \propto N_2 e^{-E_u/kT}/Z(T) , \quad (1)$$

where E_u is the energy of the upper state of the transition, N_2 is the column of warm H_2, and $Z(T)$ is the partition function. Since the levels concerned are 500–1000 K above ground, temperatures $\gtrsim 100$ K are needed for collisions to significantly excite them. Therefore, an estimate of $I_{thermal}$ can be obtained by inserting $T = 200$ K and $N_2 = 2 \times 10^{21}$ cm^{-2} (corresponding to a thickness of the emitting region of $\Delta A_v = 1$; see TH) into equation (1). We find $I_{thermal} \sim 3 \times 10^{-5}$ and 3×10^{-4} ergs s^{-1} cm^{-2} sr^{-1}, respectively for the $S(0)$ and $S(1)$ lines.

3.1.2. *The Ortho-Para Line Ratio in PDRs*

In equilibrium, at temperature T, the fraction of para-H_2 molecules, $f(p)$, is given by the statistical weights, $g(j) \equiv 2j + 1$; i.e.,

$$f(p) = \frac{\Sigma_{j=\text{even}}\, g(j) \exp(-T_j/T)}{3\Sigma_{j=\text{odd}}\, g(j) \exp(-T_j/T) + \Sigma_{j=\text{even}}\, g(j) \exp(-T_j/T)} , \quad (2)$$

where T_j is the energy of level j in K, assuming that the state-to-state deexcitation cross sections are similar. The fraction of ortho-H_2, $f(o)$, can be similarly calculated. Figure 4 shows the equilibrium ortho and para fractions graphically as a function of temperature. For $T \gtrsim 200$ K the equilibrium ortho-to-para ratio is 3, but it drops rapidly at lower temperatures, with virtually all the H_2 in the para state (i.e., with $J = 0$) for $T \lesssim 30$ K. If the molecules are formed with an ortho-to-para ratio of 3, for instance, we must determine if the ortho-to-para conversion rate is sufficiently rapid for the ratio to assume the equilibrium value given by equation (2).

There are four processes which can affect the ortho-to-para ratio of H_2. First, reactions with protons (H^+) will transform ortho into para with a rate coefficient of approximately $3 \times 10^{-10} f(p)$ cm^3 s^{-1} (Dalgarno, Black, & Weisheit 1973), assuming that the state-to-state conversion cross sections are similar (i.e., $J = 1$–0 is similar to $J = 3$–2). The corresponding reaction with H_3^+ is of lesser importance in PDRs. Second, atomic H can induce the ortho-to-para conversion, but this reaction has a considerable activation barrier. In analogy to the deuterium exchange reaction, we estimate the rate coefficient to be $1.6 \times 10^{-11} e^{(-3200/T)} f(p)$ cm^3 s^{-1}. Third, the ortho-to-para conversion can also be accomplished on grain surfaces. While in the first two cases, the ortho-para change results from a chemical exchange of a proton or H atom, in this case spin conversion results from the interaction of the nuclear spin of H_2 with the inhomogeneous magnetic field generated by unpaired electron paramagnetic impurities, radicals or lattice defects on a grain (Tielens & Allamandola 1987). The residence time of H_2 on a grain surface is sufficiently long to scan the whole grain surface and "collisions" with impurities, radicals, or defects will set the ortho-to-para ratio to the value appropriate for the grain temperature. The conversion rate is then given by the H_2 accretion rate, $8 \times 10^{-17} (T/300)^{0.5} f(p)$ cm^3 s^{-1}, where a sticking coefficient of unity has been assumed and $f(p)$ is given by equation (2), evaluated at the grain temperature. Finally, the ortho-to-para ratio can also be influ-

© American Astronomical Society • Provided by the NASA Astrophysics Data System

1992ApJ...399..563B

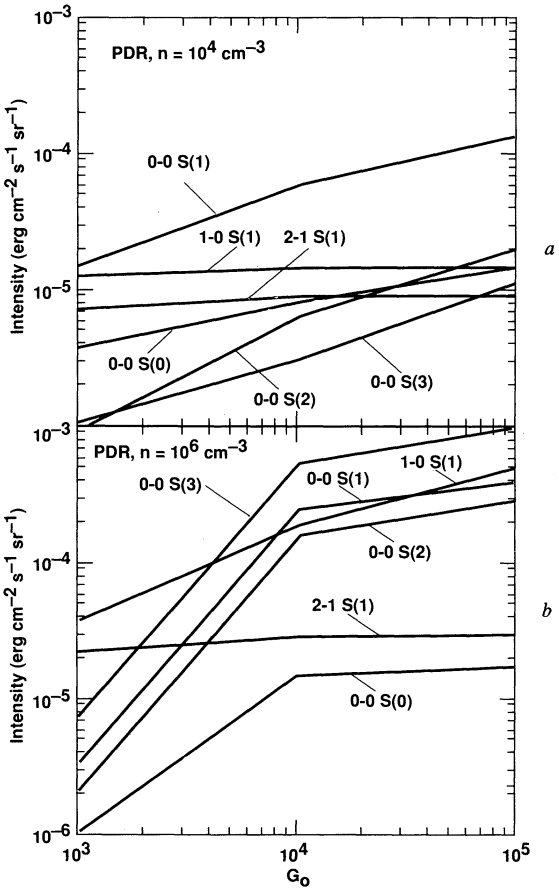

FIG. 3.—(*a*) H_2 line intensities (in ergs s^{-1} cm^{-2} sr^{-1}) for photodissociation regions with density, n, $= 10^4$ cm^{-3}, as a function of far-UV field, G_0. Shown and labeled are the $v = 0$–0 $S(0)$, $S(1)$, $S(2)$, $S(3)$, $v = 1$–0 $S(1)$ and $v = 2$–1 $S(1)$ lines. (*b*) As (*a*), but for $n = 10^6$ cm^{-3}.

enced by the H_2 formation process. In view of the large exothermicity, the initial ortho-to-para ratio of newly formed H_2 is expected to be 3. However, H_2 may not immediately evaporate upon formation but instead will diffuse across the grain surface and make ortho-para conversions in the same way that molecules accreted on to the grain convert. In that case, eventually the H_2 will thermally evaporate with an ortho-para ratio appropriate for the dust temperature. The rate in this case is given by the H_2 formation rate times the ortho or para fraction (eq. [2]) evaluated at the grain temperature.

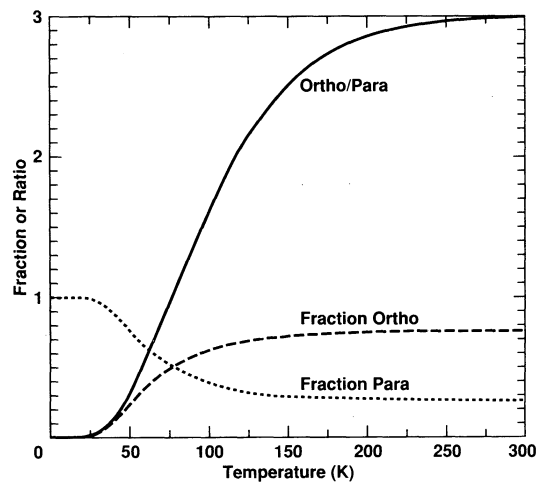

FIG. 4.—The equilibrium ortho, $f(o)$ (*long dashes*) and para, $f(p)$ (*short dashes*) fractions for H_2 as a function of temperature, calculated from eq. (2). The ortho-to-para ratio, $f(o)/f(p)$, is shown by the solid curve.

We have evaluated the ortho-para ratios for the "standard" Orion PDR model of TH ($G_0 = 10^5$, $n = 2.3 \times 10^5$ cm^{-3}) as well as for a low-density and UV-field model ($G_0 = 10^3$, $n = 10^3$ cm^{-3}; see Hollenbach, Takahashi, & Tielens 1991, hereafter HTT). In the high-density model, the gas is warm (>300 K) near the surface and ortho-para conversion by atomic H dominates, resulting in a ratio of 3. Deeper in ($A_v > 2$ mag) when the temperature drops below 300 K, gas-grain collisions take over and drive the ortho-para ratio to the equilibrium value for the dust grain temperature. For Orion ($T_{grain} \sim 75$ K), the expected ortho-para ratio is then ~ 0.9. The H_2 vibrational lines in this PDR model originate around $A_v \lesssim 2$ mag and an ortho-para ratio of 3 is therefore expected. Gas as cool as 100 K can still contribute appreciably to the lowest H_2 rotational transitions [0–0 $S(0)$ and $S(1)$; cf. Fig. 2] and thus the cool gas deeper into the PDR ($A_v > 2$ mag) will contribute, making the ortho-para ratio of these lines less than 3. In particular, with this model, we estimate that the ortho-para ratio of the two lowest rotational lines will be 1.3. The higher rotational lines originate in the warmer gas where the ortho-para ratio (equal to 3) is dominated by the H reaction.

The gas temperatures are considerably lower in the second, lower density model ($T \sim 150$ K). As a result the H exchange reaction is of little importance and the ortho-para ratio at the surface (to about the depth of the peak of H_2 vibrational emission) is set by the formation process. Deeper in, gas-grain collisions, and to a lesser extent, the H^+ exchange reaction will drive down the ratio. Assuming a formation ratio of 3, we find the ortho-para ratio to be ~ 2.5 in the vibrational H_2 emitting gas. This is also the region where the rotational lines will originate and a similar ratio is expected. On the other hand, by assuming that the formation ratio is set by the grain temperature ($T_{grain} \sim 25$ K), then nearly all the H_2 will exist in the para state.

In summary, the H_2 ortho-para ratio is a complex interplay of four different processes. For warm PDRs ($T > 300$ K), a ratio of 3 is expected in the vibrational lines, reflecting the fast exchange with atomic H at these temperatures. The lowest rotational lines originate partly from cooler gas in which the ortho-para ratio is set by gas-grain exchange. For lower density PDRs, the gas is too cool to be influenced by H exchange and now the H_2 formation process takes over at the surface. Again, gas-grain collisions dominate at higher optical depths ($A_v \gtrsim 2$). The vibrational lines as well as the lowest rotational lines originate from both zones. Since the ortho-para ratio resulting from the formation process is somewhat uncertain, it is difficult to predict the ortho-para ratio of these lines. Clearly, future observations of the ortho-para ratio of vibrational and rotational lines in a variety of PDRs can probe the interaction between H_2 and dust empirically. In the remainder of this paper we will assume an ortho-para ratio of 3 in calculating the expected intensities for the pure rotational lines. This may underestimate the intensity of the lowest para line [0–0 $S(0)$] but is likely to be accurate for observable rotational transitions originating from $J > 2$. The UV-pumped H_2 vibrational transitions may show low ortho-to-para ratios in low-density, cool PDRs if the newly formed molecules evapo-

© American Astronomical Society • Provided by the NASA Astrophysics Data System

1992ApJ...399..563B

rate from the grains after the ortho-to-para ratio has equilibrated to the grain temperature.

3.1.3. *The* CO/H_2 *Ratio in PDRs*

It has been suggested that measurement of the H_2 0–0 $S(0)$ and $S(1)$ lines and CO rotational lines with comparable excitation energies could lead to the determination of the CO/H_2 abundance ratio in PDRs (see e.g., van Dishoeck & Black 1987) Although any CO lines with $J > 7$ might be suitable, the most temperature-insensitive would be the $J = 14$–13 and 13–12 (coming from ~ 500 K above ground) to compare with the 0–0 $S(0)$ line (512 K above ground), and the $J = 17$–16 (coming from ~ 850 K above ground), to compare with the 0–0 $S(1)$ transition (850 K above the $J = 1$ level). Our models show, however, that determining the CO abundance would not be easy. First, the critical density of these CO lines is much larger ($\geq 10^5$ cm^{-3}) than for the H_2 lines and their ratio is very sensitive to density. Second, emission in the CO lines and the H_2 lines is not coextensive. The low-CO ($J \leq 10$) lines originate deeper in the cloud, typically at $A_v \sim 4$, where the C^+ transforms into C and CO. The temperature in this region is about 50 K, largely independent of density and incident UV field (TH; HTT). In contrast, the H_2 emission originates in the photoelectrically heated surface layer ($A_v \lesssim 4$), whose temperature is very sensitive to UV field and density. The high-level CO lines ($J > 10$) originate in a very thin ($\Delta A_v \sim 0.1$ mag), very warm ($T \sim 200$ K) surface layer. Again, emission in these lines is not coextensive with the H_2 line emission.

3.2. *Shocks*

3.2.1. H_2 *Line Fluxes*

The results of the J-shock model from the Hollenbach & McKee (1989) code are shown in Figure 5. The H_2 intensities are displayed as a function of shock velocity, $v_s = 5$–150 km s^{-1}, for $n_0 = 10^4$ and 10^6 cm^{-3} preshock hydrogen nucleus density.

We first discuss shocks with incomplete dissociation, $v_s \lesssim 25$–30 km s^{-1}. For $n_0 \lesssim 10^5$ cm^{-3}, the populations of postshock excited vibrational levels are subthermal, and the line ratios and intensities are sensitive to v_s. The absolute intensities in the lines also increase with n_0 for $n_0 \lesssim 10^5$ cm^{-3}; at higher densities, H_2O dominates and the absolute intensities of the lines saturate at a maximum for a given v_s. We have compared the 1–0 $S(1)$ intensities from our $n_0 = 10^4$ cm^{-3}, $v_s \leq 25$ km s^{-1} runs with those of Chang & Martin (1991), who included a much more extensive calculation of H_2 level populations behind a partially dissociative J-shock. We find agreement to better than a factor of 2. Comparison with the $n_0 = 10^6$ cm^{-3} case was not possible because Chang & Martin do not include H_2O cooling, which is dominant in our run at this high preshock density.

For $v_s \gtrsim 25$–30 km s^{-1}, the H_2 lines drop in intensity because of complete dissociation of H_2 in the hot, postshock gas. The emission at higher velocities comes from reformed molecules downstream of the shock front, and the spectrum depends on the density. Gas heating occurs due to postshock H_2 formation; at high density, the vibrationally excited molecules which have just formed are collisionally deexcited and the formation energy transformed to heat. When $n = 10^4$ cm^{-3}, the density is below critical, and the 0–0 $S(0)$, $S(1)$, and $S(2)$ lines suffer significant decline after dissociation. For $n_0 = 10^6$ cm^{-3}, however, the density is above critical and an extended column of $T \sim 400$ K gas is produced, which actually

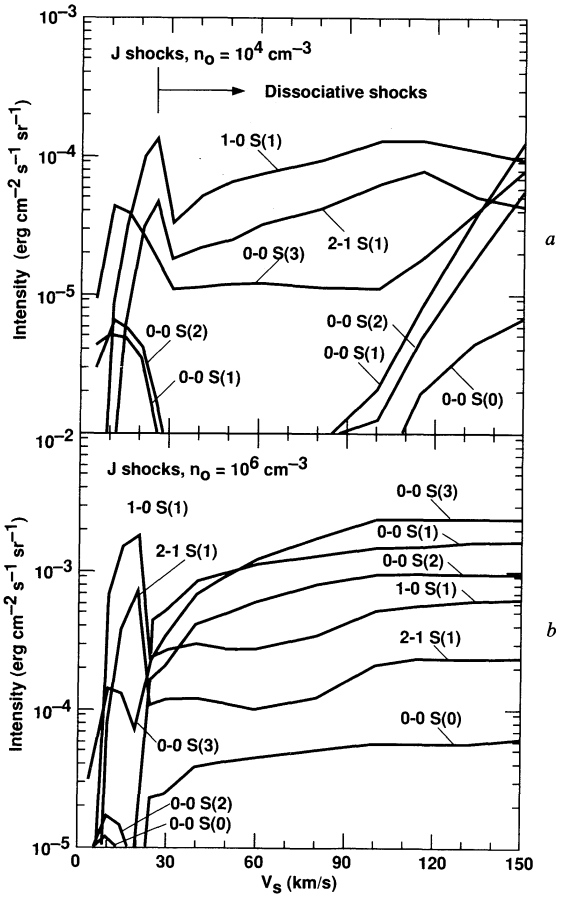

FIG. 5.—(*a*) H_2 line intensities (in ergs s^{-1} cm^{-2} sr^{-1}) in jump shocks for the $v = 0$–0 $S(0)$, $S(1)$, $S(2)$, $S(3)$, $v = 1$–0 $S(1)$ and $v = 2$–1 $S(1)$ lines, as a function of shock velocity (in km s^{-1}), for $n = 10^4$ cm^{-3}. These are calculated using the jump-shock code of Hollenbach & McKee (1989). The dissociative shock regime, $v_s \gtrsim 25$–30 km s^{-1}, is indicated. Molecule reformation occurs downstream of the shock front in this case. (*b*) As (*a*), but for $n = 10^6$ cm^{-3}.

increases the 0–0 $S(0)$, $S(1)$, $S(2)$, and $S(3)$ intensities for $v_s \gtrsim 25$ km s^{-1} (see Hollenbach & McKee 1989).

H_2 line ratios and intensities are not sensitive to v_s over much of the parameter space, for high preshock densities $n_0 \geq 10^5$ cm^{-3}. As discussed by Brand et al. (1988, 1989), the partial dissociation of H_2 for $v_s = 10$–20 km s^{-1} tends to act as a thermostat, quickly dropping postshock temperatures to ~ 3000 K, producing constant line ratios over this velocity interval, if LTE is achieved. Likewise, H_2 formation pumping and the $T = 400$ K plateau also produce relatively constant values for $v_s > 30$ km s^{-1} and $n_0 \gtrsim 10^5$ cm^{-3}. The intensity of the vibrational lines is a rapidly increasing function of velocity for $v_s \lesssim 10$ km s^{-1}, however.

Figure 6 shows the results for J-shocks with $v_s = 5$–45 km s^{-1} and $n_0 = 10^6$ cm^{-3} which ignore H_2O cooling and molecule reformation (i.e., following the Brand et al. 1988 model). Comparison with the results in Figure 5 shows that at these high densities, the presence of H_2O suppresses the overall intensities of the H_2 lines by a factor of up to ~ 10 for the lines shown. For very slow shock speeds (~ 5 km s^{-1}) the $v = 0$, low-J transitions are much stronger than the rotational-vibrational transitions, such as the 1–0 $S(1)$ line. In the "thermostat" regime, $v_s \sim 10$–20 km s^{-1}, the excitation temperature defined by the 0–0 $S(0)$ and 0–0 $S(1)$ lines is ~ 300 K,

© American Astronomical Society • Provided by the NASA Astrophysics Data System

1992ApJ...399..563B

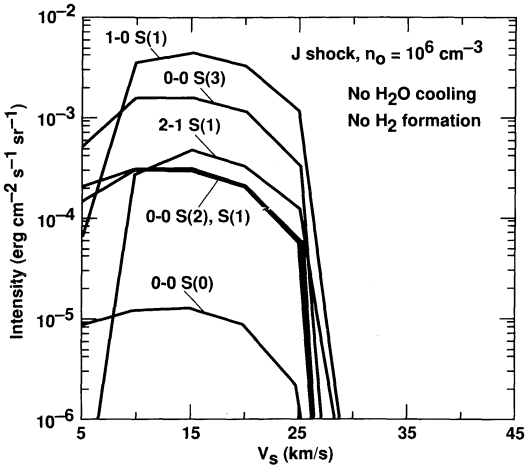

FIG. 6.—As for Fig. 5*b*, with $n = 10^6$ cm^{-3}, but for jump shocks without either H_2O included in the cooling or molecule reformation downstream of the shock front. The calculations followed the method of Brand et al. (1988) to fit the near-IR line emission from OMC-1.

whereas, for instance, that defined by the 1–0 *S*(1) and 2–1 *S*(1) lines is ~2000 K. The *S*(1)/*S*(0) excitation temperature is somewhat higher than that derived for PDR emission, but the vibrational excitation temperature for shocks is considerably less than the 5000–10,000 K temperature (due to UV pumping) derived for low-density ($n \lesssim 10^4$ cm^{-3}) PDRs.

For comparison purposes, we display the C-shock results from Draine et al. (1983) for the same preshock conditions and $v_s = 5$–45 km s^{-1} in Figure 7. One key difference in the C-shock results is that the intensities of the vibrational lines are more sensitive to v_s over a larger region of parameter space ($v_s = 5$–30 km s^{-1}). The peak postshock temperature in the C-shocks increases with shock velocity up to temperatures of order 3000–4000 K ($v_s \sim 40$ km s^{-1} for the models run), where the H_2 dissociates and the C-shock breaks down into a dissociative J-shock. Another key difference is that the absolute intensity of the vibrational H_2 lines can attain higher values, because the C-shock can produce larger columns of 2000 K gas. For the slowest shock speeds, $v_s \sim 5$ km s^{-1}, the low-J H_2 lines are considerably reduced in the C-shock model compared to the Brand et al. model, due to the presence of CO and [O I] 63 μm cooling suppressing the emission in these lines.

3.2.2. *The Ortho-to-Para Ratio in Shocks*

It should be emphasized that the above shock results assumed a fixed ortho-to-para abundance ratio of 3 throughout the emitting region. Since the preshock gas is presumably cold ($\lesssim$50 K), the ortho-to-para ratio in the preshock gas could be much less than 3, if the ortho-to-para conversion time in the molecular cloud is less than the cloud lifetime. However, in many cases, the hot postshock gas will rapidly convert para to ortho through H exchange (see § 3.1.2) and quickly establish the high-temperature ($T > 200$ K) ratio of ortho to para of 3. Therefore the observer will measure a ratio of 3. We have compared the conversion time scale with the cooling time scale in shocks and derived the following results. In fast, dissociative J-shocks, most of the H_2 emission derives from formation pumping and from collisional excitation in the H_2 formation temperature plateau ($T \sim 400$ K) (Hollenbach & McKee 1989). In the former case, the ortho-to-para ratio is 3 if newly formed molecules rapidly escape from the grain surface (see § 3.1.2). In the latter case, the ortho-to-para ratio is 3. In slow, nondissociative J-shocks, the para-H_2 will convert to ortho-H_2 only if the atomic hydrogen abundance x_H is greater than about 0.01 to 0.1. This will occur in 15–25 km s^{-1} shocks, where partial dissociation occurs, but is not likely in slower 5–10 km s^{-1} molecular J-shocks. Such slow J-shocks, if they exist, may show strong para lines but weak ortho transitions. In C-shocks, the conversion depends on the peak neutral temperature, T_{max}, achieved in the shock and the atomic hydrogen abundance. If $T_{max} > 1000$ K, so that vibrational H_2 emission is significant, we find that conversion occurs if $x_H \gtrsim 10^{-4}(x_i/10^{-6})$, where x_i is the ionic abundance. This condition is likely to be satisfied so that ortho/para ratios should be 3 in these C-shocks. However, if $T_{max} \sim 300$ K, so that mainly pure H_2 rotational emission is excited, then conversion only occurs if $x_H \gtrsim 0.1(x_i/10^{-6})$. This is not likely, and the para 0–0 *S*(0) and *S*(2) line emission may dominate in such C-shocks.

3.2.3. *The CO-to-H_2 Ratio in Shocks*

We have examined the problem of determining the CO/H_2 abundance ratio by measuring CO and H_2 rotational lines which originate at very similar excitation energies above ground. If the lines are optically thin and the levels are in LTE, the ratio of such lines will be nearly independent of density and temperature (i.e., shock structure) and will determine the abundance ratio provided that the ratio does not change through the shock. The latter requirement rules out dissociative shocks,

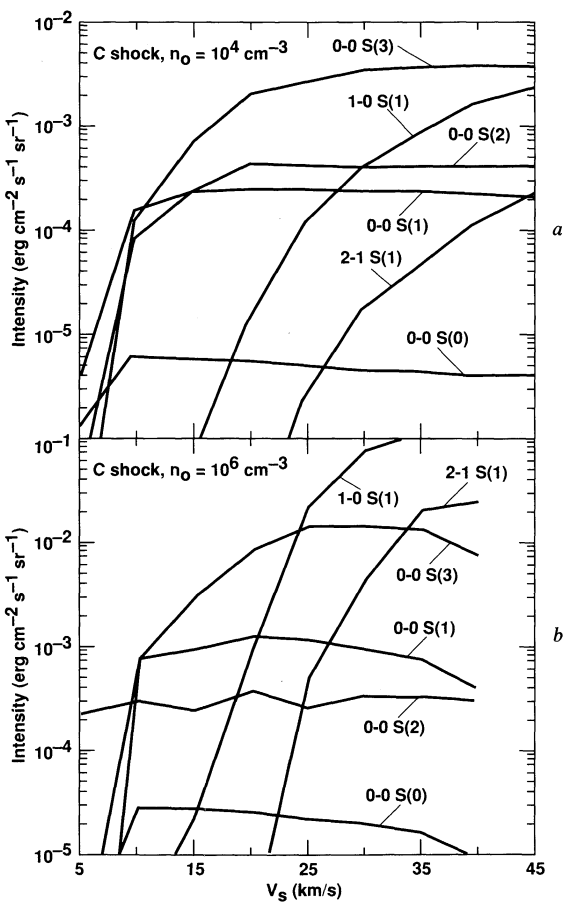

FIG. 7.—As for Fig. 5, but for nondissociative continuous shocks (from Draine, Roberge, & Dalgarno 1983). For faster shock velocities, the H_2 molecule dissociates and the shock becomes a jump shock.

© American Astronomical Society • Provided by the NASA Astrophysics Data System

1992ApJ...399..563B

since CO tends to dissociate downstream from H_2 and to reform upstream of H_2. However, in nondissociative molecular shocks, all the gas phase hydrogen is H_2 and all the gas phase carbon tends to be in CO throughout the emitting region of the shock. In this case, the analytic solution to optically thin, LTE cooling gives

$$\frac{I\{H_2[0\text{–}0\ S(0)]\}}{I[\mathrm{CO}(14\text{–}13)]} \sim 1.9 \times 10^{-6} \frac{n(H_2)}{n(\mathrm{CO})} e^{70/T} \quad (3)$$

$$\frac{I\{H_2[0\text{–}0\ S(1)]\}}{I[\mathrm{CO}(17\text{–}16)]} \sim 1.0 \times 10^{-4} \frac{n(H_2)}{n(\mathrm{CO})} e^{5/T} . \quad (4)$$

Note that for $T > 100$ K there is virtually no temperature dependence. These results agree well with the nondissociative J-shock model for $n \gtrsim 10^5$ cm^{-3}, so that the appropriate CO levels are in LTE. C-shocks with sufficient density to put CO into LTE may produce optically thick CO lines, however. In summary, it is not trivial to obtain the CO/H_2 abundance ratio from shock emission; the effects of non–LTE and self-absorption in the CO lines, as well as the differential dissociation and reformation of these molecules, makes the determination of the abundance ratio best suited only to dense ($n_0 \gtrsim 10^5$ cm^{-3}), nondissociative ($v_s \lesssim 20$ km s^{-1}) J-shocks.

4. APPLICATIONS

4.1. H_2 *Rotational Lines from the Orion PDR*

The line emission from the lowest ortho (odd-J) and para (even-J) transitions of H_2 arises from warm gas at temperatures of 100–300 K, comprising a significant fraction of the gas in molecular clouds. The lines are optically thin and come from the dominant species present in the gas, and thus provide a powerful tool to explore these regions in the Galaxy. Since these lines are not very density sensitive, their intensity is an excellent probe of the column density of warm molecular gas, and their ratio can be used to measure the temperature of the gas.

Parmar et al. (1991) have recently detected emission from the 0–0 $S(1)$ and 0–0 $S(2)$ lines from the Orion Bar PDR. This is the first time the 0–0 $S(1)$ line had been observed. Over a $10'' \times 16''$ region of the Bar, they measured an intensity of $\sim 7 \times 10^{-4}$ and $\sim 5 \times 10^{-4}$ ergs s^{-1} cm^{-2} sr^{-1} in the $S(1)$ and $S(2)$ lines, respectively. This corresponds to a kinetic gas temperature of about 450 K (see Fig. 1) and a column density of warm H_2 of 1.3×10^{21} cm^{-2} (see Fig. 2). Tielens & Hollenbach (1985b) and BHT have modeled the PDR in the Orion Bar. The atomic fine structure ([O I], [C II], [Si II]), CO rotational and H_2 vibrational emission from this region imply a clumpy medium, containing gas with $n \sim 10^5$ cm^{-3} and 90% surface filling factor, surrounding high-density, $n \sim 10^7$ cm^{-3} clumps, with 10% surface filling factor, all irradiated by a FUV field, $G_0 = 10^5$, produced by the Trapezium star cluster. The rotational H_2 line emission is dominated by the lower density ($\sim 10^5$ cm^{-3}) material, and the models predict temperatures of ~ 500 K in that gas. Although we get good agreement in the temperature, the calculated intensities emerging from the *front* surface are about 50% of those measured. Undoubtedly, this reflects on the edge-on appearance of the Orion Bar rather than the face-on geometry assumed in the calculation. The prediction for the 0–0 $S(0)$ line intensity is 4×10^{-5} ergs s^{-1} cm^{-2} sr^{-1}, taking the geometry into account.

4.2. H_2 *Rotational Lines from the Orion Shock*

The brightest H_2 emission line source in the sky, by an order of magnitude, is the shock in the OMC-1, in Orion (e.g., Beckwith et al. 1978). Here, a nondissociating shock wave is being driven by a fast wind, probably from the source IRc2, into the surrounding molecular cloud at 10–40 km s^{-1} (e.g., Genzel & Stutzki 1989). It is of interest to determine whether the 0–0 $S(0)$ line will be detectable in this source. Since there is some doubt about which shock models actually represent the near-IR emission observed (see discussion earlier), we shall present the results of the C-shock models of Draine et al. (1983) and the J-shock models summarized in this paper. Since the absolute column density of the shocked gas is uncertain (e.g., through the geometry), line ratios will be used for the comparison. These intensity ratios also depend on the differential extinction between 2.1 μm and the mid-IR lines, and we assume $A_K = 1$–2 mag with $A_\lambda \propto \lambda^{-1.7}$. Table 3 lists the intensity ratio predictions of these models, together with the measured line ratios (corrected for differential extinction) inferred from the intensity measurements of the 0–0 $S(1)$ and $S(2)$ lines at Peak 1 of OMC-1 (P. S. Parmar & J. H. Lacy, private communication). In the table, we include the J-shock model fit to the Peak 1 H_2 line emission of Brand et al. (1988) (col. [3]), and the C-shock model fit of Draine & Roberge (1982) (col. [4]), as well as some representative results from J- (cols. [5] and [6]) and C- (cols. [7] and [8]) shock models discussed in this paper.

There are large differences in the predictions between the J- and C-shock models of Brand et al. and Draine and Roberge, with the J-shock being closer to the measured intensities. This results partly from the neglect of H_2O cooling in the J-shock model, which increases the low-J H_2 emission of the shock. It also reflects partly the rather high near-IR extinction ($A_K = 4$ mag) adopted by Draine & Roberge. This value is now believed to be somewhat smaller (e.g., $A_K \sim 1$ mag, as adopted by Brand et al.). In order to fit the resulting high intrinsic 1–0 $S(1)$ line intensities, a large shock velocity is required, and such a C-shock will have a low ratio of pure rotational line intensities to the 1–0 $S(1)$ line (cf. Fig. 5). For a lower near-IR foreground extinction, a better fit to the observation with a C-shock model is perhaps possible with a lower shock velocity (e.g., see cols. [7] and [8] of Table 3).

The results from a nondissociative J-shock model with (col. [6]) and without (col. [5]) H_2O cooling are also shown. It is clear that with H_2O cooling such models cannot match the observations; the ratios of 0–0 $S(0)$/1–0 $S(1)$ and 0–0 $S(2)$/1–0 $S(1)$ are an order of magnitude smaller than the observed values. The H_2O cooling reduces the column of warm (~ 200 K) gas which produces the 17 and 12 μm lines. The absolute intensities of the lines are also too small, but, as mentioned above, we place less emphasis on the absolute intensities since the area filling factors of the shocks are very uncertain.

The Brand et al. (1988) model of a J-shock with no H_2O cooling (col. [3]) does match the data. It has the attractive feature that the predicted line ratios are rather insensitive to n_0, if $n_0 \gtrsim 10^5$ cm^{-3}, so that LTE is achieved, and to v_s for $10 \lesssim v_s \lesssim 20$ km s^{-1}. C-shock models also apparently fit the data (e.g., col. [8]) if the shock velocities are close to the breakdown velocity in which H_2 dissociation occurs, and a C-shock transforms into a J-shock. Smith & Brand (1990) have recently proposed that numerous fast bow shocks in the beam may produce a spectrum which is dominated by that portion of the bow shock in which the normal velocity component produces a C-shock near breakdown.

© American Astronomical Society • Provided by the NASA Astrophysics Data System

1992ApJ...399..563B

TABLE 3

PREDICTIONS FOR ROTATIONAL LINE RATIOS AT PEAK 1 OF OMC-1

Line Ratio (1)	Observed Ratio[a] (2)	J Model Fit[b] (3)	C Model Fit[c] (4)	J-Shock[d] ($n = 10^6$ cm^{-3}, $v_s = 15$ km s^{-1}) (5)	J-Shock[e] ($n = 10^6$ cm^{-3}, $v_s = 15$ km s^{-1}) (6)	C-Shock[f] ($n = 10^6$ cm^{-3}, $v_s = 25$ km s^{-1}) (7)	C-Shock[f] ($n = 10^4$ cm^{-3}, $v_s = 40$ km s^{-1}) (8)
0–0 $S(0)$/1–0 $S(1)$	...	9.8 (−3)	1.9 (−4)	2.9 (−3)	1.6 (−4)	1.1 (−3)	2.6 (−3)
0–0 $S(1)$/1–0 $S(1)$	0.15–0.06	1.1 (−1)	6.4 (−3)	6.9 (−2)	6.3 (−3)	5.5 (−2)	1.4 (−1)
0–0 $S(2)$/1–0 $S(1)$	0.23–0.09	1.1 (−1)	1.6 (−2)	6.7 (−2)	1.0 (−2)	1.3 (−2)	2.5 (−1)
0–0 $S(3)$/1–0 $S(1)$	...	4.4 (−1)	1.5 (−1)	3.6 (−1)	8.7 (−2)	6.5 (−1)	2.2
1–0 $S(1)$[g]	0.021–0.054	2.1 (−2)	3.4 (−1)	4.5 (−3)	1.5 (−3)	2.0 (−2)	1.6 (−3)

[a] Intrinsic line ratio, correcting the observed intensities for the differential extinction between the emitting wavelengths. It is assumed that $A_\lambda \propto \lambda^{-1.7}$, and that the extinction at 2.1 μm ranges from 1 to 2 mag. The 0–0 $S(1)$ and 0–0 $S(2)$ lines were measured to be $3.3 \pm 0.6 \times 10^{-3}$ and $5.0 \pm 0.1 \times 10^{-3}$ ergs s^{-1} cm^{-2} sr^{-1} through a 4″ aperture (P. S. Parmar & J. H. Lacy, private communication). The 1–0 $S(1)$ intensity measured through a 5″ aperture is 8.5×10^{-3} ergs s^{-1} cm^{-2} sr^{-1} (Brand et al. 1988). In calculating the ratios, no correction for the difference in aperture size between the measurements has been applied.

[b] Intrinsic line ratio, following the model fit to Peak 1 from Brand et al. 1988 and Burton et al. 1989b. In this model the intensities were normalized to match the observed 1–0 $S(1)$ line intensity, assuming the extinction at 2.1 μm is 1 mag.

[c] Intrinsic line ratio, following the model fit to Peak 1 from Draine & Roberge 1982. In this model the intensities were normalized to match the observed 1–0 $S(1)$ line intensity, assuming the extinction at 2.1 μm is 4 mag.

[d] Intrinsic line ratio, following the J-shock model of Brand et al. 1988 (i.e., nondissociative, no H_2O cooling).

[e] Intrinsic line ratio, following the J-shock model of Hollenbach & McKee 1989 (i.e., nondissociative, with H_2O cooling).

[f] Intrinsic line ratio, following the C-shock model of Draine, Roberge, & Dalgarno 1983.

[g] For the 1–0 $S(1)$ line, intensities in ergs s^{-1} cm^{-2} sr^{-1} are listed across the page instead of line ratios, and a beam filling factor of unity is assumed in cols. (5)–(8).

4.3. H_2 *Rotational Lines and ISO*

The launch of the *Infrared Satellite Observatory* (*ISO*) is imminent. *ISO* will have the ability to measure the 17 and 28 μm lines free of atmospheric absorption and the thermal background associated with earth based platforms. Expected sensitivities for 5 σ detections in 1 hr observing are $\sim 10^{-5}$ ergs s^{-1} cm^{-2} sr^{-1} (R. Genzel, private communication). Inspection of Table 2 and the figures suggests that we will then be able to detect regions of extended emission in these lines for PDRs with $G_0 \gtrsim 10^4$, and in shocks where the preshock density is $\gtrsim 10^5$ cm^{-3}.

In PDRs, however, there is significant continuum emission in the mid-IR from dust grains, with contributions from dust thermal emission and transiently heated small particles (see HTT). The dust temperature at $A_v \sim 1$, where one finds the bulk of the warm molecular gas, is $\sim$35, 55, and 90 K for $G_0 = 10^3$, 10^4, and 10^5, respectively, increasing as the FUV field rises. Taking the predictions of HTT, and extrapolating to the measured values in the Orion Bar (Becklin et al. 1976), we may estimate the continuum emission at these wavelengths, for comparison with the line emission. With the spectral resolving power of 20,000 for the Fabry-Perot etalon on the short-wavelength spectrometer in *ISO*, we predict line to continuum ratios for the 28 μm line of $\sim$2 for $G_0 = 10^3$, $\sim$0.7 for $G_0 = 10^4$, and $\sim$0.1 for $G_0 = 10^5$. For the 17 μm line, these ratios are typically an order of magnitude greater. We do not expect to be able to detect the lines when $G_0 \leq 10^3$ (too weak), but paradoxically, although the line intensity is greater for stronger FUV fields, the 0–0 $S(0)$ line may prove easier to detect in moderate FUV fields simply because the line to continuum ratio decreases with increasing G_0. There should be no difficulty in detecting the 0–0 $S(1)$ line against the continuum, and the larger flux compared to the 0–0 $S(0)$ line makes this line much the easier to detect of the pair. Figure 8 summarizes the results for the 0–0 $S(0)$ 28 μm line and the 0–0 $S(1)$ 17 μm line. The $S(0)$ line intensity is relatively insensitive to G_0 or n for $G_0 \geq 10^3$ and $n \geq 10^3$ cm^{-3}. The $S(1)$ line, however, significantly increases in intensity with increasing n and G_0 for $10^3 \leq n \leq 10^7$ and $10^3 \leq G_0 \leq 10^5$. The line-to-continuum ratio for both lines decreases with increasing G_0.

At the location of the OMC-1 shock, observations of the 0–0 $S(0)$ line will have to contend with the strong mid-IR continuum emission from the BN-KL IR nebula. On Peak 1, we estimate that this will amount to $\sim$100 Jy in the 14″ × 20″ *ISO* beam. Taking the observed 1–0 $S(1)$ line intensity measured in a 20″ aperture to be 3.5×10^{-11} ergs s^{-1} cm^{-2} (Burton et al. 1988), then we would predict that the 0–0 $S(0)$ line intensity will be $\sim 1 \times 10^{-4}$ ergs s^{-1} cm^{-2} sr^{-1} in the slow J-shock model, and $\sim 3 \times 10^{-5}$ ergs s^{-1} cm^{-2} sr^{-1} in the C-shock model (see cols. [3] and [4] of Table 3). If one-third of the line flux falls in the central resolution element (with $\Delta v = 15$ km s^{-1}), then the line-to-continuum ratio will be 0.4 for a J-shock, readily observable, and 0.1 for a C-shock, a somewhat harder observation.

5. CONCLUSIONS

The fundamental ortho and para transitions of the hydrogen molecule are the 0–0 $S(1)$ and 0–0 $S(0)$ lines, at 17 and 28 μm, respectively. We have modeled the emission from these lines, as well as the 0–0 $S(2)$, 0–0 $S(3)$, 1–0 $S(1)$, and 2–1 $S(1)$ lines, in photodissociation regions and in shocks. In PDRs we find that detectable intensities of the 0–0 $S(0)$ and 0–0 $S(1)$ lines are produced from thermally excited molecular gas at temperatures of 100–300 K, situated at optical depths $A_v \gtrsim 1$ from the neutral surface of the clouds. As such, they provide a powerful probe of the warm molecular gas in the Galaxy in an optically thin line. In shocks, the lines can be detected from lower velocity interactions than previously observed and might provide a diagnostic between competing models of shock excitation.

The 0–0 $S(0)$ and $S(1)$ lines are hard to detect from Earth-based platforms due to the high thermal background and poor atmospheric transmission. We predict that the *ISO* satellite should be able to detect these lines in regions where the FUV radiation field, $G_0 \gtrsim 10^4$. In both cases, the 0–0 $S(1)$ line will be very much easier to detect than the 0–0 $S(0)$ line due to its

© American Astronomical Society • Provided by the NASA Astrophysics Data System

1992ApJ...399..563B

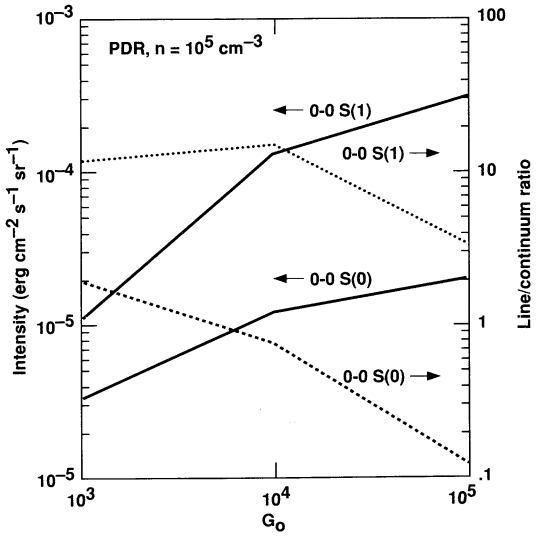

FIG. 8*a*

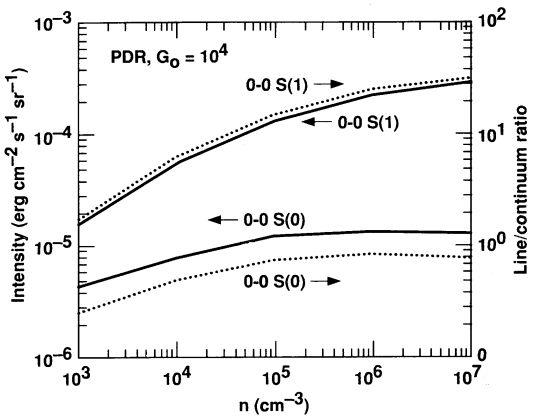

FIG. 8*b*

FIG. 8.—(*a*) Intensities and line to continuum ratio for the $v = 0$–0 $S(0)$ and $v = 0$–0 $S(1)$ lines as a function of far-UV field, G_0, for a PDR with $n = 10^5$ cm^{-3}. The left-hand axis shows the intensity and the right-hand axis, the predicted line-to-continuum ratio, for a spectral resolution of 20,000. Line intensities are connected by solid lines, and the line-to-continuum ratios, by dotted lines. (*b*) As (*a*), but this time as a function of density, n with the far-UV field held fixed at $G_0 = 10^4$.

greater brightness, and much higher line-to-continuum ratio. In fact, the 0–0 $S(0)$ line may prove to be easier to detect in regions with moderate FUV fields ($G_0 \sim 10^4$) due to the high dust continuum brightnesses at 28 μm in stronger FUV fields. Measurements of the relative line ratios in shocks may be used to discriminate between competing models for molecular cloud shocks. However, we do not expect that comparison with the intensities of high-J CO lines will readily lead to a direct determination of the CO/H_2 abundance ratio. The H_2 ortho-to-para ratio for these lines is hard to accurately predict, due to uncertainty about the ortho-to-para conversion processes. Future observations of the ortho-to-para ratio with the low rotational H_2 lines may allow us to probe the interactions between H_2 molecules and dust grains in the ISM.

We are grateful for several stimulating discussions with R. Genzel, J. Spynromilio, and A. Sternberg, and to J. Lacy and P. Parmar for also letting us use their results in advance of publication. We should like to thank the Astronomy/Relativity branch at NASA Headquarters for their support under NASA RTOP 188-44-53 and under a special theory program which supports a joint Center for Star Formation Studies at NASA/Ames Research Center, U.C. Berkeley, and U.C. Santa Cruz.

REFERENCES

Becklin, E. E., Beckwith, S., Gatley, I., Matthews, K., Neugebauer, G., Sarazin, C., & Werner, M. W. 1976, ApJ, 207, 770
Beckwith, S., Persson, S. E., Neugebauer, G., & Becklin, E. E. 1978, ApJ, 223, 464
Black, J. H., & van Dishoeck, E. F. 1987, ApJ, 322, 412
Brand, P. W. J. L., Moorhouse, A., Burton, M. G., Geballe, T. R., Bird, M., & Wade, R. 1988, ApJ, 334, L103
Brand, P. W. J. L., Toner, M. P., Geballe, T. R., Webster, A. S., Williams, P. M., & Burton, M. G. 1989, MNRAS, 236, 929
Burton, M. G., Brand, P. W. J. L., Geballe, T. R., & Webster, A. S. 1989a, MNRAS, 236, 409
Burton, M. G., Brand, P. W. J. L., Moorhouse, A., & Geballe, T. R. 1989b, in Infrared Spectroscopy in Astronomy, ed. B. H. Kaldeich (Proc. 22nd ESLAB Symposium [ESA SP-290]), 281
Burton, M. G., Geballe, T. R., Brand, P. W. J. L., & Webster, A. S. 1988, MNRAS, 231, 617
Burton, M. G., Hollenbach, D. J., Haas, M. R., & Erickson, E. F. 1990a, ApJ, 355, 197
Burton, M. G., Hollenbach, D. J., & Tielens, A. G. G. M. 1990b, ApJ, 365, 620 (BHT)
Chang, C. A., & Martin, P. G. 1991, ApJ, 378, 202
Chernoff, D. F., Hollenbach, D. J., & McKee, C. F. 1982, ApJ, 259, L97
Dabrowski, I. 1984, Canadian J. Phys., 62, 1639
Dalgarno, A., Black J. H., & Weisheit, J. C. 1973, Astrophys. Lett., 14, 77
Draine, B. T. 1980, ApJ, 241, 1021
———. 1991, in IAU Symp. 147, Fragmentation of Molecular Clouds and Star Formation, ed. E. Falgarone, F. Boulanger, & G. Duvert (Dordrecht: Kluwer), 185
Draine, B. T., & Roberge, W. G. 1982, ApJ, 259, L91
Draine, B. T., Roberge, W. G., & Dalgarno, A. 1983, ApJ, 264, 485
Flower, D. R., Pineau des Forêts, G., & Hartquist, T. W. 1985, MNRAS, 216, 775
Genzel, R., & Stutzki, J. 1989, ARA&A, 27, 41
Habing, H. J. 1968, Bull. Astron. Inst. Netherlands, 19, 421
Hollenbach, D. J., Chernoff, D. F., & McKee, C. F. 1989, in Infrared Spectroscopy in Astronomy, ed. B. H. Kaldeich (Proc. 22nd ESLAB Symposium [ESA SP-290]), 245
Hollenbach, D., & McKee, C. F. 1989, ApJ, 342, 306
Hollenbach, D. J., & Shull, J. M. 1977, ApJ, 216, 419
Hollenbach, D. J., Takagashi, T., & Tielens, A. G. G. M. 1991, ApJ, 377, 192 (HTT)
Kwan, J. 1977, ApJ, 216, 713
London, R., McCray, R., & Chu, S.-I. 1977, ApJ, 217, 442
Neufeld, D. A., & Melnick, G. J. 1987, ApJ, 322, 266
Parmar, P. S., Lacy, J. H., & Achtermann, J. M. 1991, ApJ, 372, L25
Smith, M. D. 1991, MNRAS, 253, 175
Smith, M. D., & Brand, P. W. J. L. 1990, MNRAS, 243, 498
Sternberg, A., & Dalgarno, A. 1989, ApJ, 338, 197
Tielens, A. G. G. M., & Allamandola, L. J. 1987, in Interstellar Processes, ed. D. Hollenbach & H. Thronson (Dordrecht: Reidel), 397
Tielens, A. G. G. M., & Hollenbach, D. J. 1985a, ApJ, 291, 722 (TH)
———. 1985b, ApJ, 291, 747
Turner, J., Kirby-Docken, K., & Dalgarno, A. 1977, ApJS, 35, 281
van Dishoeck, E. F., & Black, J. H. 1987, in Physical Processes in Interstellar Clouds, ed. G. E. Morfill & M. Scholer (Dordrecht: Reidel), 241

© American Astronomical Society • Provided by the NASA Astrophysics Data System